



# CHORUS

This is the accepted manuscript made available via CHORUS. The article has been published as:

## Surface Modes of Coherent Spinodal Decomposition

Ming Tang (✉) and Alain Karma

Phys. Rev. Lett. **108**, 265701 — Published 26 June 2012

DOI: [10.1103/PhysRevLett.108.265701](https://doi.org/10.1103/PhysRevLett.108.265701)

# Surface Modes of Coherent Spinodal Decomposition

Ming Tang (唐铭)

*Condensed Matter and Materials Division, Lawrence Livermore National Laboratory,  
Livermore, CA 94550, USA*

Alain Karma

*Department of Physics and Center for Interdisciplinary Research on Complex Systems,  
Northeastern University, Boston, MA 02115, USA*

Abstract:

We use linear stability theory and numerical simulations to show that spontaneous phase separation in elastically coherent solids is fundamentally altered by the presence of free surfaces. Due to misfit stress relaxation near surfaces, phase separation is mediated by unique surface modes of spinodal decomposition that have faster kinetics than bulk modes and are unstable even when spinodal decomposition is suppressed in the bulk. Consequently, in the presence of free surfaces, the limit of metastability of supersaturated solid solutions of crystalline materials is shifted from the coherent to chemical spinodal.

Spinodal decomposition is a ubiquitous phase separation process leading to the spontaneous formation of domain structures with distinct chemical compositions in diverse systems ranging from metallic alloys to polymers to liquids. The seminal work of Cahn and Hilliard [1,2] laid down the theoretical foundation for understanding the mechanism of this important phenomenon in bulk materials. On the phase diagram of a binary system with a miscibility gap, there is a limit of metastability inside which the solid solution becomes unstable against infinitesimal

composition fluctuations and spontaneously decomposes into a two-phase structure. Such a process, known as spinodal decomposition, leads to periodic composition variations of a definite wavelength that is governed by the competition between the destabilizing chemical free energy and the stabilizing composition gradient energy as well as the elastic energy that can arise due to the coupling of composition and stress. When phase separation does not generate internal stress (e.g. in liquids and some glass), the metastability limit of bulk solid solution is defined by the *chemical spinodal* within which the second derivative of the chemical free energy density  $f$  against composition  $c$  is negative ( $\partial^2 f / \partial c^2 < 0$ ). However, spinodal decomposition in most crystalline solids gives rise to coherency stress due to the variation of lattice parameter  $a$  with composition:  $\varepsilon = d \ln a / dc \neq 0$ . The incurred elastic energy suppresses phase separation and shifts the metastability limit to the *coherent spinodal* curve at lower temperatures on the phase diagram, as illustrated in Figure 1. Cahn [2] showed that the coherent spinodal is defined by the condition  $\partial^2 f / \partial c^2 + 2\varepsilon^2 Y' = 0$ , where  $Y'$  is an elastic constant. The supercooling from the chemical to the coherent spinodal can vary from several to several hundred Kelvins in different systems.

In this Letter, we address the fundamental question: how does the presence of free surfaces alter spinodal decomposition in elastically coherent solids? Because internal stress can be relieved in the proximity of free surfaces, intuition suggests that coherent spinodal decomposition should develop more easily near a surface than in the bulk. This scenario is supported by several recent phase-field simulations [3-5] that show preferential domain formation along surfaces of thin films during decomposition. Domain structure of similar morphology has also been seen in experiments [6, 7]. However, despite a vast body of research on phase separation in crystalline solids in the literature (e.g. see ref. 8), how surfaces influence

spinodal decomposition is not quantitatively understood beyond this intuitive picture, thereby making it difficult to interpret experimental observations. Here we use linear stability theory to show unambiguously that there exists unique surface modes of coherent spinodal decomposition (SCSD) that develop under conditions where spinodal decomposition does not occur in the bulk. A major finding is that the unstable region of the crystalline solid solution is not bound by the coherent but the chemical spinodal when free surfaces are present in the system, and SCSD can become the dominant phase separation mechanism in the region between the chemical and coherent spinodals. We expect SCSD to be especially important in nanostructures, in which the surface area to volume ratio is very high and bulk spinodal decomposition may even be suppressed [9,10].

It is important to distinguish between SCSD and other surface-mediated spinodal decomposition phenomena where the surface energy plays a dominant role. Spinodal decomposition may be initiated at a surface wall when one component of a binary mixture is preferentially attracted to the wall [11], or when the surface energy favors demixing [12]. In a more complex setting, spinodal decomposition localized at an alloy-electrolyte interface has been invoked to explain nanoporosity formation during dealloying [13]. In contrast, the surface localization in SCSD is due solely to stress relaxation; it is independent of the surface energy which neither drives the instability nor selects its wavelength. Hence, SCSD also differs fundamentally from other types of stress-driven surface instabilities [14] where the surface energy is instrumental in determining the pattern scale.

We consider a two-dimensional semi-infinite solid under plane strain condition with a flat surface at  $z=0$  and the  $x$  axis parallel to the surface. The solid has two components A and B, and  $c(x,z)$  is the local molar composition. Stress can be represented by the Airy stress function

$\Gamma(x, z)$ :  $\sigma_{xx} = \partial_z^2 \Gamma$ ,  $\sigma_{zz} = \partial_x^2 \Gamma$ ,  $\sigma_{xz} = -\partial_x \partial_z \Gamma$ . The system is assumed to be isotropic and elastically homogeneous, and its stress-free strain due to composition variation follows Vegard's law:  $\varepsilon_{ij}^*(c) = \varepsilon_0 c \delta_{ij}$  ( $i, j = x, z$ ), where  $\varepsilon_0$  is the misfit strain between pure A and B. We express the system's free energy as  $F = \iiint [f(c) + f_{elas} + \kappa/2(\nabla c)^2] dV + \iint \gamma dA$ , where  $f(c)$  is the chemical free energy density,  $f_{elas} = 1/2 \sigma_{ij}(\varepsilon_{ij} - \varepsilon_{ij}^*(c))$  the linear elastic energy,  $\kappa$  the gradient energy coefficient, and  $\gamma$  the surface energy. We assume  $\gamma$  to be independent of composition and stress, and neglect the surface energy effect that is shown in ref. 15 to be negligible in comparison to the elastic and chemical energies associated with a small composition modulation.

The evolution of the composition field follows the Cahn-Hilliard equation [2]

$$\partial_t c = M \Delta [-\kappa \Delta c + f'(c) + f_{elas}'(c)] \quad (1)$$

where  $M$  is the mobility, the prime denotes a derivative,  $\Delta \equiv \partial_x^2 + \partial_z^2$  and

$f_{elas}'(c) = -\varepsilon_0 (\sigma_{xx} + \sigma_{zz}) = -\varepsilon_0 \Delta \Gamma$ . The elasticity equilibrium is governed by

$$\Delta^2 \Gamma = -\frac{E \varepsilon_0}{1 - \nu^2} \Delta c \quad (2)$$

where  $E$  and  $\nu$  are the Young's modulus and Poisson ratio, respectively. To analyze the stability

of a spatially uniform state  $c = c_0$  against small perturbations, we linearize the equations about

that state, i.e.  $f'(c) \approx f'(c_0) + f''(c_0)(c - c_0)$ , define the scaled fields  $\phi = c - c_0$  and  $\Phi = \Gamma \varepsilon_0 / \kappa$ ,

and normalize the equations with length unit  $l_0 = \sqrt{(1 - \nu^2) \kappa / E \varepsilon_0^2}$  and time unit  $t_0 = l_0^4 / M \kappa$ .

After linearization and normalization, Eqs. 1-2 become

$$\left[ \partial_t + \Delta(\Delta + k_0^2 - 1) \right] \phi = 0 \quad (3)$$

$$\Delta^2 \Phi + \Delta \phi = 0 \quad (4)$$

Note that  $\Phi$  is eliminated from Eq. 3 using Eq. 4. The governing equations are complemented by boundary conditions at the surface,

$$\partial_z \left[ (\Delta + k_0^2) \phi + \Delta \Phi \right] \Big|_{z=0} = \partial_z \phi \Big|_{z=0} = 0 \quad (5,6)$$

$$\partial_x^2 \Phi \Big|_{z=0} = \partial_x \partial_z \Phi \Big|_{z=0} = 0 \quad (7,8)$$

Eqs. 5 and 6 impose the conditions of zero concentration flux and gradient across the surface as employed in ref. 3-5 for composition-independent surface energy, and Eqs. 7 and 8 are the traction-free boundary conditions. The only parameter appearing in Eqs. 3-8,

$$k_0 = \sqrt{-f''(c_0) / [E\varepsilon_0^2 / (1-\nu^2)]},$$

characterizes the strength of the chemical driving force of phase separation relative to the elastic energy;  $k_0=1$  and  $0$  define the bulk coherent and chemical spinodal curves on a phase diagram, respectively. When a system resides within the coherent spinodal, i.e.  $k_0 > 1$ , the amplitude of a bulk plane-wave composition perturbation of the form  $\phi \propto \exp(i\vec{k} \cdot \vec{r} + \omega^{\text{bulk}} t)$  either grows or decays with time as  $\exp(\omega^{\text{bulk}} t)$ , where the amplification factor  $\omega^{\text{bulk}}$  is a function of wave vector  $k$ :  $\omega^{\text{bulk}}(k) = k^2(k_0^2 - 1 - k^2)$ . A bulk perturbation is unstable if its  $k$  is below a critical value  $k_{\text{crit}}^{\text{bulk}} = \sqrt{k_0^2 - 1}$ , which approaches zero at the coherent spinodal. The spinodal decomposition kinetics in the early stage is dominated by the fastest-growing mode with  $k = k_m \equiv \sqrt{(k_0^2 - 1) / 2}$  and  $\omega = \omega_m \equiv k_m^4$ .

Let us now analyze the stability of a supersaturated solid solution against a *surface-localized* composition perturbation of the form  $\phi \propto \exp(ikx - qz + \omega t)$ , which is periodic parallel to the surface but decays exponentially into the bulk ( $\text{Re}[q] > 0$ ). Substituting this ansatz for  $\phi$  into Eq. 3, one obtains  $q^2 = k^2 - k_m^2 \pm i\sqrt{\omega - \omega_m}$ . Depending on the value of  $\omega$ , the decay constant  $q$

admits different solutions, which results in different forms of surface-mode perturbations [15].

The most important ones are:

- i) For  $\omega > \omega_m$ ,  $q$  is complex; the composition and stress fields of the surface modes, whose expressions are given in ref. 15, have an “underdamped” form that exhibits spatially decaying oscillation in the  $z$  direction.
- ii) For  $\omega < \omega_m$ ,  $q$  is real; the surface perturbations are free of oscillation in the  $z$  direction and are referred to as “overdamped” with the expressions given in ref. 15.

Six unknown constants, denoted as  $\alpha_i$  ( $i=1,2$ ) and  $\beta_j$  ( $j=1-4$ ), appear in the solutions of  $\phi$  and  $\Phi$  for the above surface eigenmodes, to be determined from the initial and boundary conditions. By substituting  $\phi$  and  $\Phi$  into Eqs. 3-8, we find that  $\alpha_{1,2}$  and  $\beta_{1-4}$  must satisfy six linear equations, which in matrix form are  $\mathbf{M}(k, \omega; k_0) [\alpha_1, \alpha_2, \beta_1, \beta_2, \beta_3, \beta_4]^T = \mathbf{0}$  [15]. As a necessary condition to have non-trivial surface modes, the determinant of the coefficient matrix  $\mathbf{M}$  must equal zero, i.e.  $\text{Det}[\mathbf{M}] = 0$ . This condition implicitly determines the dispersion relation  $\omega = \omega^{\text{surf}}(k)$  for surface-mode perturbations, which is controlled by the single parameter  $k_0$  that encapsulates the effects of all thermodynamic and materials parameters. Figure 2 shows the calculated  $\omega^{\text{surf}}(k)$  curves at several  $k_0$  values, which represent different regions on the phase diagram that have distinct phase separation behaviors:

- 1) *Within the bulk coherent spinodal* ( $k_0 > 1$ ), spinodal decomposition occurs via both surface and bulk modes but the surface mode has a larger growth rate. As illustrated in Figure 2(a) for  $k_0 = 1.1$ , all surface perturbations with  $k < k_b$  are underdamped and have larger growth rates than the most unstable bulk mode with an amplification factor  $\omega_m$ . The overdamped section ( $\omega < \omega_m$ ) of the  $\omega^{\text{surf}}(k)$  curve connects smoothly to the underdamped section at  $k = k_b$  where  $\omega^{\text{surf}}(k_b) = \omega_m$ .

The fastest-growing surface mode,  $\omega^{\text{surf}} = \omega_{\text{max}}^{\text{surf}}$ , occurs at a non-zero wave vector  $k_{\text{max}}^{\text{surf}}$ . By

Taylor expansion of  $\text{Det}[\mathbf{M}]$  around  $\omega=0$ , we found that the root of  $\omega^{\text{surf}}(k)$  is determined by

$$\frac{k}{k_m^2} \left[ (k^2 + k_m^2 + 2k_m^4) \sqrt{k^2 - 2k_m^2 - k^3} \right] = 0 \quad (9)$$

It is straightforward to derive from Eq. 9 that the critical wave vector of the surface modes,  $k_{\text{crit}}^{\text{surf}}$ , is smaller than  $k_{\text{crit}}^{\text{bulk}}$ . These results unequivocally confirm that the stress relaxation near free surfaces enhances the instability of finite-wavelength perturbations and results in faster phase separation kinetics than in the bulk. In the long wavelength limit  $k \rightarrow 0$ , however, the real part of  $q$  of underdamped modes approaches zero. The perturbation thus extends into the bulk in this limit and behaves like a bulk mode with  $\omega^{\text{surf}} \rightarrow \omega_m$  [15].

2) *In between the coherent and chemical spinodals* ( $0 < k_0 < 1$ ), surface-mode perturbations with  $k < k_{\text{crit}}^{\text{surf}}$  continue to be unstable even though bulk spinodal decomposition is now suppressed, as shown in Figure 2(a) for  $k_0=0.85$ . However, different from the case of  $k_0 > 1$ , the surface modes now become overdamped in the vicinity of  $k=0$  and  $\omega^{\text{surf}}$  approaches zero upon  $k \rightarrow 0$ . The solid is thus metastable against long-wavelength overdamped modulations, which is an important distinction between overdamped and underdamped surface modes. This region can be further divided into two subregions [15]. When  $1 > k_0 > k_0^* \approx 0.7246$ , surface perturbations including the most unstable mode are underdamped at intermediate wavelengths  $k_{b2} < k < k_{b1}$  and overdamped otherwise. For  $k_0^* > k_0 > 0$ , however, the underdamped modes cease to exist and all surface perturbations assume the overdamped form, see Figure 2(b). The boundary line separating the two subregions, defined by  $k=k_0^*$ , is plotted in Figure 1. When the system moves from the

coherent towards the chemical spinodal ( $k_0=0$ ),  $k_{\text{crit}}^{\text{surf}}$  is decreased and fewer surface modes are unstable. Upon  $k_{\text{crit}}^{\text{surf}}$  reaching zero, the crystalline solid becomes metastable against any surface-mode perturbations. Mathematically, this happens when  $k=0$  becomes a double root of  $\omega^{\text{surf}}(k)$ , which is found from Eq. 9 to occur only at  $k_0=0$ , i.e. exactly on the chemical spinodal. Therefore, *the chemical spinodal is also the surface coherent spinodal*, which is the metastability limit of supersaturated crystalline solid solution with free surfaces. By expanding  $\text{Det}[\mathbf{M}]$  in series around  $k_0=\omega=k=0$ , we find that  $\omega^{\text{surf}}(k)$  in the limit  $k_0 \rightarrow 0$  has the asymptotic expression  $4k^2(k_0^2 - 2k^2)/3$ , or  $4Mk^2[-f''(c_0) - 2\kappa k^2]/3$  in dimensional units. Remarkably, this result shows that the kinetics of SCSD becomes asymptotically independent of elastic energy when approaching the chemical spinodal. This is because upon  $k_0 \rightarrow 0$ , the unstable overdamped surface perturbations have diverging wavelengths. Under this limit, the incurred elastic energy makes an increasingly small contribution relative to the chemical and gradient energies and its effect on SCSD diminishes asymptotically. Despite being stress independent,  $\omega^{\text{surf}}(k)$  upon  $k_0 \rightarrow 0$  is different from the dispersion relation of stress-free chemical spinodal decomposition in the bulk,  $\omega^{\text{chem}}(k) = k^2(k_0^2 - k^2)$ . Such difference stems from the different spatial composition variations of surface and bulk chemical eigenmodes.

3) *In between the chemical spinodal and the miscibility gap* (pure imaginary  $k_0$ ),  $\omega^{\text{surf}}(k) \leq 0$  for all  $k$  (e.g.  $k_0=0.5i$  in Figure 2(a)), and the system is metastable against infinitesimal composition perturbations.

Additional physical insights into surface modes can be obtained by analyzing the dependence of the critical wavelength in physical units,  $\Lambda_C \equiv 2\pi l_0 / k_{\text{crit}}^{\text{surf}}$ , on the chemical driving force

measured by  $k_0$ .  $\Lambda_c$  can be computed analytically in two limits. First, at the bulk coherent spinodal ( $k_0=1$ ), the solid is marginally stable against bulk fluctuations but has unstable surface modes with a critical wavevector  $k_{\text{crit}}^{\text{surf}} = \sqrt{3}/2$  [15], yielding

$$\Lambda_c(k_0 = 1) \equiv \Lambda_c^* = 4\pi\sqrt{(1-v^2)\kappa/3E\varepsilon_0^2} \quad (10)$$

Eq. (10) makes the key prediction that in the vicinity of the bulk coherent spinodal, the characteristic length scale of surface modes is solely determined by the misfit strain, elastic modulus, and coefficient  $\kappa$  that determines the chemical energy cost of compositional modulations. For typical parameter values, this length is on the nanoscale as shown below.

Second, the asymptotic form of  $\omega^{\text{surf}}(k)$  for  $k_0 \ll 1$  implies that the critical wavelength diverges as  $\Lambda_c(k_0) \approx \sqrt{3/2}\Lambda_c^*/k_0$  near the chemical spinodal. In between the two limits, the simple formula,  $\Lambda_c(k_0) \approx \Lambda_c^*\sqrt{(3-k_0^2)/2k_0^2}$ , which interpolates between the above asymptotically exact results for  $k_0=1$  and  $k_0 \ll 1$ , gives a remarkably good prediction of the critical wavelength over the whole range  $0 < k_0 \leq 1$  as shown in Fig. S1 [15]. This formula generally predicts how to tune the wavelength of surface modes by varying thermodynamic conditions and material properties.

We confirmed the linear stability analysis results with numerical simulations by solving Eqs. 1-2 with free-surface boundary conditions. The simulation domain has two free surfaces at  $z=0$  and 200 nm that are sufficiently separated apart, and periodic boundary condition is applied in the  $x$  direction. The system is modeled as a regular solution, i.e.,

$f(c) = a[c \ln c + (1-c) \ln(1-c)] + bc(1-c)$ , with the following parameters:  $a = 0.19T \text{ J/cm}^3$  ( $T$  - temperature in K),  $b=274 \text{ J/cm}^3$ ,  $\kappa=5 \times 10^{-12} \text{ J/cm}$ ,  $E=100 \text{ GPa}$ ,  $v=0.25$ ,  $\varepsilon_0=0.05$ , and  $M=10^{-12} \text{ cm}^5/\text{J}\cdot\text{s}$ . For those parameters,  $\Lambda_c^*=9.9 \text{ nm}$ . Figure 1 is the phase diagram for such a model

system. Figure 3(a) shows the snapshots of the decomposition process from an initial state at  $c_0 =$

0.5 and  $T=298\text{K}$  plus a small random fluctuation, corresponding to a dimensionless  $k_0=1.1$  (Figure 2(a)). Consistent with the theory, phase separation first occurs in the surface region and produces a lateral domain pattern aligned with the surface. Only at much later times does an isotropic domain structure emerge from bulk spinodal decomposition. In Figure 3(b), the amplitude of the dominant surface composition wave,  $A_{\text{max}}^{\text{surf}}(t)$ , displays exponential growth with time at the early stage that agrees well with the theoretically predicted  $\exp(\omega_{\text{max}}^{\text{surf}} t)$ . Deviation of  $A_{\text{max}}^{\text{surf}}(t)$  from theory becomes pronounced at later times due to the nonlinear term in Eq. 1. We calculated  $\omega_{\text{max}}^{\text{surf}}$  numerically as a function of  $k_0$  from a series of simulations at different initial states. As shown in Figure 3(c), the numerical values are in very good agreement with the linear theory. We note that the parameters employed in the simulations are comparable to those used for studying phase separation kinetics in a lithium-ion insertion electrode material  $\text{Li}_x\text{FePO}_4$  [16,17], in which a Li-rich ( $\text{LiFePO}_4$ ) and Li-poor ( $\text{FePO}_4$ ) phase is separated by a miscibility gap.  $\text{FePO}_4/\text{LiFePO}_4$  domains aligned along the surface were observed in thin plate particles in a previous experiment [7], suggesting that they probably result from SCSD. Such a connection is corroborated by more detailed 3D simulations that account for the anisotropies of Li diffusion and elasticity in  $\text{LiFePO}_4$ , to be published elsewhere.

Our finding on the existence of SCSD has profound implications for the stability and microstructural evolution of phase-separating crystals. Many important engineering materials such as ternary III-V semiconductors [18] show a large separation between the chemical and coherent spinodals due to strong misfit strain energy. SCSD considerably expands the unstable region of the homogeneous solution of these materials and may control the phase separation morphology. The development of lateral composition modulation has been frequently seen in semiconductor and magnetic thin films grown epitaxially on substrates [6,19]. Although phase

separation in such films is affected by both the free surface and substrate/film interface, the epitaxial strain usually favors composition homogeneity [20], but the stress relaxation near surface promotes lateral fluctuation. Notably, Hsieh et al. [6] observed a depth-dependent composition modulation in low-temperature grown  $\text{Al}_{0.3}\text{Ga}_{0.7}\text{As}$  films after annealing at  $600^\circ\text{C}$ . The lateral Al concentration variation is most pronounced near the surface and decays gradually into the films, which bears close resemblance to the surface-mode perturbations. While a vacancy-assisted mechanism was suggested by Hsieh et al. to account for the depth dependence, the well-defined orientation and periodicity of the domain pattern is a strong indication of the occurrence of SCSD during annealing.

In summary, we have revealed the existence of unique surface modes of coherent spinodal decomposition (SCSD) in crystalline solids with miscibility gaps and derived analytical predictions for their characteristic wavelength. SCSD exhibits larger growth rates than the bulk modes and extends the instability region of a supersaturated solid solution from the coherent to the chemical spinodal. SCSD generates heterostructures with very different morphology and feature sizes from bulk spinodal decomposition, which may be potentially utilized in a variety of applications such as nanostructure patterning and photoluminescence. Our study and its extension will provide guidance for controlling SCSD to produce desired nanostructures.

The work of M. T. is performed under the auspices of the US Department of Energy by Lawrence Livermore National Laboratory under Contract DE-AC52-07NA27344. Support from the Laboratory Directed Research and Development (LDRD) Program is acknowledged. A. K. acknowledges support of DOE grant DEFG02-07ER46400. Simulations were carried at the National Energy Research Scientific Computing Center, which is supported by the Office of Science of the U.S. Department of Energy under Contract No. DE-AC02-05CH11231.

## References

1. J. W. Cahn and J. E. Hilliard, *J. Chem. Phys.* **28**, 258 (1958).
2. J. W. Cahn, *Acta Metall.* **9**, 795, 1961.
3. D. J. Seol, S. Y. Hu, Y. L. Li, J. Shen, K. H. Oh, and L. Q. Chen, *Metal Mater. Int.* **9**, 61 (2003).
4. D. J. Seol, S. Y. Hu, Y. L. Li, J. Shen, K. H. Oh, and L. Q. Chen, *Acta Mater.* **51**, 5173 (2003).
5. S. M. Wise, J. S. Kim, and W. C. Johnson, *Thin Solid Films* **473**, 151 (2005).
6. K. C. Hsieh et al., *Appl. Phys. Lett.* **68**, 1790 (1996).
7. G. Y. Chen, X. Y. Song, and T. J. Richardson, *Electrochem. Solid State Lett.* **9**, A295 (2004).
8. P. Fratzl, O. Penrose, and J. L. Lebowitz, *J. Stats. Phys.* **95**, 1429 (1999).
9. J. J. Hoyt, *Acta Mater.* **57**, 1105 (2009).
10. H. P. Fischer, P. Maass, and W. Dieterich, *Europhys. Lett.* **42**, 49 (1998).
11. S. Puri, *J. Phys.: Condens. Matter* **17**, R101 (2005).
12. H. P. Fischer, P. Maass, and W. Dieterich, *Phys. Rev. Lett.* **79**, 893 (1997).
13. J. Erlebacher et al., *Nature* **410**, 450 (2001).
14. R. J. Asaro and W. A. Tiller, *Metall. Trans.* **3**, 1789 (1972); M. A. Grinfeld, *Sov. Phys. Dokl.* **31**, 831 (1987); D. J. Srolovitz, *Acta Metall.* **37**, 621 (1989).
15. See Supplemental Material online for additional information.
16. M. Tang, W. C. Carter, and Y.-M. Chiang, *Annu. Rev. Mater. Res.* **40**, 469 (2010).
17. M. Tang, J. F. Belak, and M. R. Dorr, *J. Phys. Chem. C* **115**, 4922 (2011).
18. G. B. Stringfellow, *J. Electron. Mater.* **11**, 903 (1982).

19. I. S. Yu et al., Phys. Rev. B **82**, 035308 (2010).

20. W. C. Johnson and C. S. Chiang, J. Appl. Phys. **64**, 1155 (1988).

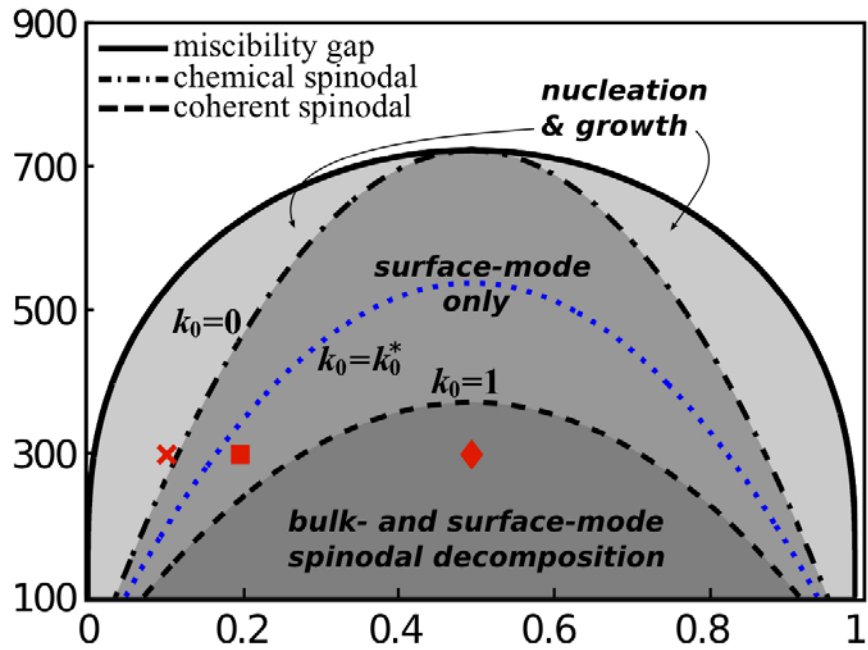


Figure 1 Phase diagram of a regular solution solid modeled after parameters described in the text. Areas of different shades represent regions in which phase separation occurs through different mechanisms. The dotted line denotes the existence limit of underdamped surface modes. The states marked by the symbols  $\blacklozenge$  ( $k_0=1.1$ ),  $\blacksquare$  ( $k_0=0.85$ ), and  $\times$  ( $k_0=0.5i$ ) correspond to the  $\omega^{\text{surf}}(k)$  curves plotted in Figure 2(a).

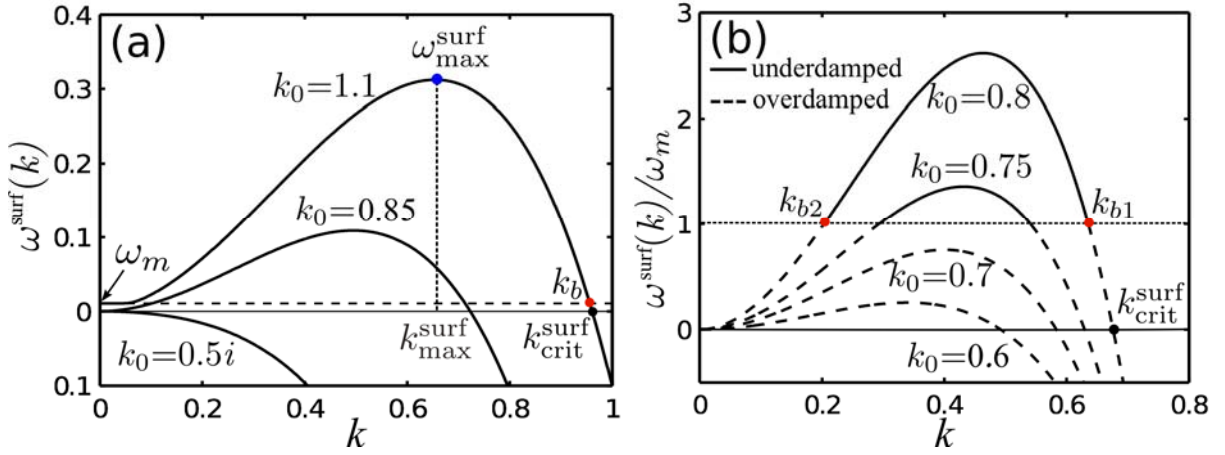


Figure 2 (a) Dispersion relation  $\omega^{\text{surf}}(k)$  of SCSD at  $k_0=1.1, 0.85$  and  $0.5i$  in dimensionless units. (b)  $\omega^{\text{surf}}(k)$  normalized by  $\omega_m$  at  $k_0=0.8, 0.75, 0.7$  and  $0.6$ . Underdamped ( $\omega^{\text{surf}} > \omega_m$ ) and overdamped ( $\omega^{\text{surf}} < \omega_m$ ) surface modes are represented by solid and dashed lines, respectively.

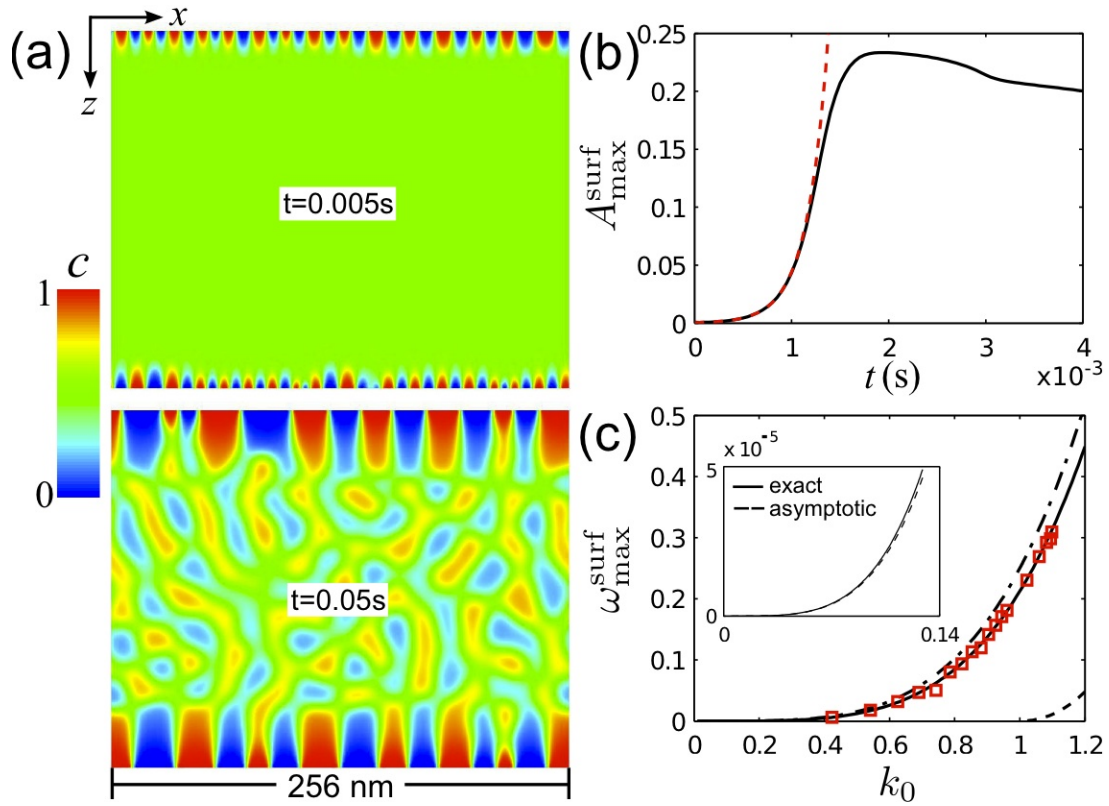


Figure 3 (a) Snapshots of spinodal decomposition in a solid with free surfaces and an initial state at  $c_0 = 0.5$  and  $T=298\text{K}$  ( $\blacklozenge$  in Figure 1). (b) Amplitude of the dominant surface composition wave calculated from simulation (solid) and linear stability analysis (dashed). (c) Dimensionless  $\omega_{\text{max}}^{\text{surf}}$  vs.  $k_0$  calculated from simulations (squares) and linear theory (solid line). Also shown are the maximal  $\omega$  of bulk coherent (dashed) and chemical (dashed-dotted) spinodal decomposition. The inset compares the asymptotic and exact expressions of  $\omega_{\text{max}}^{\text{surf}}(k)$  in the limit  $k_0 \rightarrow 0$ .